Asociación Argentina
de Mecánica Computacional

Mecánica Computacional Vol XXXI, págs. 3789-3796 (artículo completo)
Alberto Cardona, Paul H. Kohan, Ricardo D. Quinteros, Mario A. Storti (Eds.)
Salta, Argentina, 13-16 Noviembre 2012

EFFECTS OF CASSON RHEOLOGY ON ANEURYSM WALL SHEAR STRESS

Marcelo A. Castro[a,d], **María C. Ahumada Olivares**[b], **Christopher Putman**[c], **Juan Cebral**[d]

[a] *CONICET, Grupo de Investigación y Desarrollo en Bioingeniería, Facultad Regional Buenos Aires, UTN, Medrano 951, Buenos Aires, Argentina, marcelo.a.castro@gmail.com, http://sites.google.com/site/marceloadriancastro*

[b] *Universidad Favaloro, Facultad de Ingeniería, Ciencias Exactas y Naturales, Solís 453, Buenos Aires, Argentina*

[c] *Department of Interventional Neuroradiology, Inova Fairfax Hospital, 3300 Gallows Rd., Falls Church, Virginia, USA*

[d] *Department of Computational and Data Sciences, George Mason University, 4400 University Blvd., Fairfax, Virginia, USA, jcebral@gmu.edu, http://cfd.gmu.edu/~jcebral*

Keywords: Cerebral aneurysms, Wall shear stress, Numerical simulations, Non-newtonian

Abstract. It is widely accepted that wall shear stress plays an important role in cerebral aneurysm initiation, progress and rupture. Previous works have shown strong evidence in support of the high wall shear stress as a risk factor associated to those biomechanical processes. Patient-specific image-based computational hemodynamic modeling of vascular systems harboring cerebral aneurysms has demonstrated to be a fast and reliable way to compute quantities difficult or impossible to be measured in-vivo. The accuracy of the simulation results have been successfully validated in the past. Additionally, most model assumptions have shown no impact on the flow characterization whose association with the mentioned processes was investigated. Particularly, the incorporation of the blood rheology in large arterial systems containing aneurysms resulted in similar hemodynamic characterizations for most aneurysms. However, large aneurysms, especially those containing blebs are expected to have flow rates in the range where Newtonian and non-Newtonian models exhibit the largest differences. In order to study the impact of blood rheology in vascular systems harboring specific intracranial aneurysms, unsteady finite element blood flow simulations were carried out over patient-specific models. Those models were reconstructed from rotational angiographic images using region growing and deformable model algorithms. Unstructured finite element meshes were generated using and advancing front technique. Walls were assumed as rigid, traction-free boundary conditions were imposed at the outlets of the models, and a flow rate wave form was imposed at the inlets after scaling according to the Murray's Law for optimal arterial networks. The Casson model was incorporated as a velocity gradient dependent apparent viscosity and the results were compared to those using the Newtonian rheology. Regions with differentiated wall shear stress values and orientations were studied.

1 INTRODUCTION

Image-based patient-specific blood flow numerical simulations have been used for more than a decade to investigate possible associations between hemodynamic characteristics and evolution of cerebrovascular pathologies like the initiation, growth and rupture of cerebral aneurysms (Taylor et al., 1998; Steinman et al., 2003; Cebral et al., 2005; Castro et. al, 2009). Most cerebral aneurysms appear in the Circle of Willis, located at the base of the brain. There is agreement about the role of wall shear stress (WSS) in the formation, growth and ultimately rupture of cerebral aneurysms (Nakatani et al., 1991; Crompton et al., 1996).

During the last years some research groups have investigated the correlation between hemodynamic characteristic and initiation, development and rupture of cerebral aneurysms using numerical simulations. A previous study showed a possible association between high maximum WSS at the systolic peak and rupture in a cohort of AComA aneurysms (Castro et al., 2006). In a large study including 210 cerebral aneurysms at different locations it was found a statistical significant association between rupture and WSS distributions with elevated maximum WSS, high flow concentration and small impingement size (Cebral et al., 2011). Cebral et al. also showed a connection between location of aneurysm blebs and regions of high WSS in models where blebs were virtually removed (Cebral et al., 2010). In another study, it was presented a relationship between rupture, and coexistence of high WSS and high positive spatial WSS gradient, observed in three-patient scanned before and after aneurysm formation (Kulcsar et al., 2011). Although other investigators reported possible associations between low shear stress and either rupture (Jou et al., 2008; Shojima et al., 2004) or blister formation (Shojima et al., 2010), most experimental, clinical and numerical evidence suggest a connection between high WSS values and aneurysm formation. Particularly, the 20 vascular models harboring aneurysms in the middle cerebral artery reconstructed in Shojima et al., 2004, considered a limited portion of the parent artery, neglecting important features of the vascular geometry that resulted in a simplified simulated blood flow. Later, it was demonstrated that such simplifications significantly alter intra aneurysmal flow patterns (Castro et al., 2006).

Although most previous computational studies assumed that blood behaves as a Newtonian fluid, this assumption may not be completely accurate under some hemodynamic conditions. WSS in idealized models of saccular aneurysms was studied using Casson rheology under different flow conditions (Low et. al, 1993; Khanafer et al., 2006; Fisher et al., 2009). Particularly, Khanafer et al. showed that non-Newtonian wall shear stress is greater during the peak systole in aortic aneurysm models. A limited number of patient-specific studies have been presented. Rayz et al. found no significant differences between low wall shear stress regions that may be associated with risk of thrombus formation using Newtonian and non-Newtonian computational fluid dynamic simulations in three patients (Rayz et al., 2008). However, accounting for non-Newtonian behavior improved the agreement with observations using longitudinal MRI studies. Xiang et al. showed that Newtonian viscosity model could overestimate normalized wall shear stress and consequently underestimate the risk of rupture of intracranial aneurysm in three internal carotid artery saccular aneurysms (Xiang et al., 2012). These results would suggest a dependence of WSS distributions on the real vascular geometry.

The purpose of this work is to compare the WSS values and orientation in patient-specific cerebral aneurysm models containing blebs where low flow is expected, using both Newtonian and Casson rheology in order to investigate regions of underestimation and overestimation of WSS in realistic geometries.

2 METHODS

2.1 Vascular imaging and modeling

Two patients with cerebral aneurysms containing blebs were selected from our data base. Three dimensional rotational angiography images were acquired using a Philips Integris System (Philips Medical Systems, Best, The Netherlands). Each 8-second acquisition consisted in 120 projections obtained during a 180° rotation, which were reconstructed into a 3D dataset of 128^3 voxels covering a field of view of 54.02 mm on a dedicated workstation. The voxel resolution was therefore 0.422 mm. These data were exported into a PC for mathematic vascular modeling using a previously presented methodology (Yim et al., 2002; Cebral et al., 2005; Castro et al., 2006). High-quality volumetric finite element grids composed of tetrahedral elements with an advancing front technique were generated for each case (Löhner et al., 1996a; Löhner et al., 1996b; Löhner et al., 1997). Element size was adjusted in order to approximately maintain the same number of elements in both large and small arteries. A minimal mesh resolution of 0.16 mm was prescribed for internal carotid arteries, which resulted in grids containing up to 2.5 million tetrahedra.

2.2 Blood flow numerical simulations

Finite element blood flow numerical simulations were performed using both Newtonian and non-Newtonian Casson rheologies. For the Newtonian case, blood was modeled as an incompressible fluid with attenuation 1.0 g/cm^3 and viscosity 0.04 Poise. For the Casson model a velocity dependent apparent gradient derived from that non-Newtonian model is computed at every mesh node (1)

$$\mu_{app} = \left(\sqrt{\tau_0 \frac{1 - e^{-m\dot{\gamma}}}{\dot{\gamma}}} + \sqrt{\mu} \right)^2 \tag{1}$$

where τ_0 is the yield stress, which was assumed as 0.09 dyn/cm^2, μ is the Newtonian viscosity and $\dot{\gamma}$ is the shear strain rate. The exponent m, which is assumed greater that 10, is included in order for the apparent viscosity to be bonded for any range of shear strain rates (Pham et al., 1994).

The governing equations were the unsteady Navier-Stokes equations in 3D (Mazumdar, 1992). Vessel walls were assumed rigid, and no slip boundary conditions were applied at the walls. Pulsatile flow conditions derived from PCMR measurement in healthy subjects were imposed at the inlet of the models. Flow waveforms were scaled with the inlet area to achieve a mean WSS of 15 dyn/cm^2 at the inflow boundary of each model. This choice is consistent with studies relating vessel area and flow rates in internal carotid and vertebral arteries (Cebral et al., 2008), as well as with the principle of minimal work expressed by Murray's law (Sherman, 1981). Fully developed pulsatile velocity profiles were prescribed with use of the Womersley solution (Womersley, 1955; Taylor et al., 1998). Assuming that all distal vascular beds have similar total resistance to flow, traction-free boundary conditions with the same pressure level were applied at outlet boundaries. The Navier-Stokes equations were numerically integrated by using a fully implicit finite-element formulation (Cebral et al., 2005). Two cardiac cycles using 100 time-steps per cycle were computed, and all of the results reported correspond to the second cardiac cycle.

2.3 Wall shear stress analysis

Maps of WSS magnitude were created to visualize the distribution of shear forces on the aneurysm wall for both Newtonian and Casson rheologies. The percent relative difference between both distributions was computed. Additionally, the angular difference of WSS vector orientations was also calculated. Above mentioned maps were compared in order to establish possible correlations and determine the impact of blood rheology on the underestimation or overestimation of WSS. Intraaneurysmal WSS was not normalized with respect to the parent artery values. Instead, normalization was achieved by scaling the mean flow rate inflow waveform using the cross-sectional area according to the principle of minimal work expressed by Murray's law (Sherman, 1981).

3 RESULTS

Two vascular images exhibiting large aneurysms were selected from our data base. The first one (Case #1) corresponds to a patient with a two-lobulation aneurysm. The second one (Case #2) has multiple blebs on the aneurysm wall. Cross-sectional area of the internal carotid artery was computed for both cases: 0.119 cm^2 (Case #1) and 0.160 cm^2 (Case #2). Those areas where used to scale the flow rates previously acquired using phase-contrast magnetic resonance imaging in a normal volunteer in order to meet the criterion of minimal biological work for a typical mean WSS of 15 dyn/cm^2 at that artery (Sherman, 1981; Castro et al., 2008, Cebral et al. 2008). The scaled curves are shown in Figure 1.

The first two columns in Figure 2 correspond to Case #1, and the last two columns, to Case #2. Vascular models were reconstructed from rotational angiography images (Figure 2a-d). Maps of absolute value of WSS for both Newtonian rheology (Figure 2e-h) and Casson rheology (Figure 2i-l) were created. The same color map was used for all maps with a maximum WSS value of 50 dyn/cm^2 (magenta). The relative difference between absolute values of WSS for Newtonian and Casson flows was computed (Figure 2m-p). Color maps range between blue (where the Newtonian WSS is as much as twice the Casson WSS) to magenta (where the Casson WSS is as much as twice the Newtonian WSS). Dark regions correspond to similar WSS values. Finally, the angle between the coplanar WSS vectors at each mesh node was computed, ranging from 0° to 20° for the first case, and from 0° to 12° for the second case (Figure 2q-t).

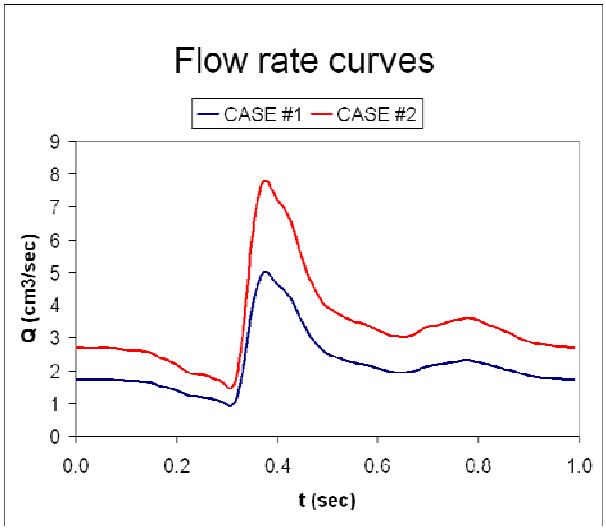

Figure 1: Flow rate curves imposed at the internal carotid artery of Case #1 and Case #2.

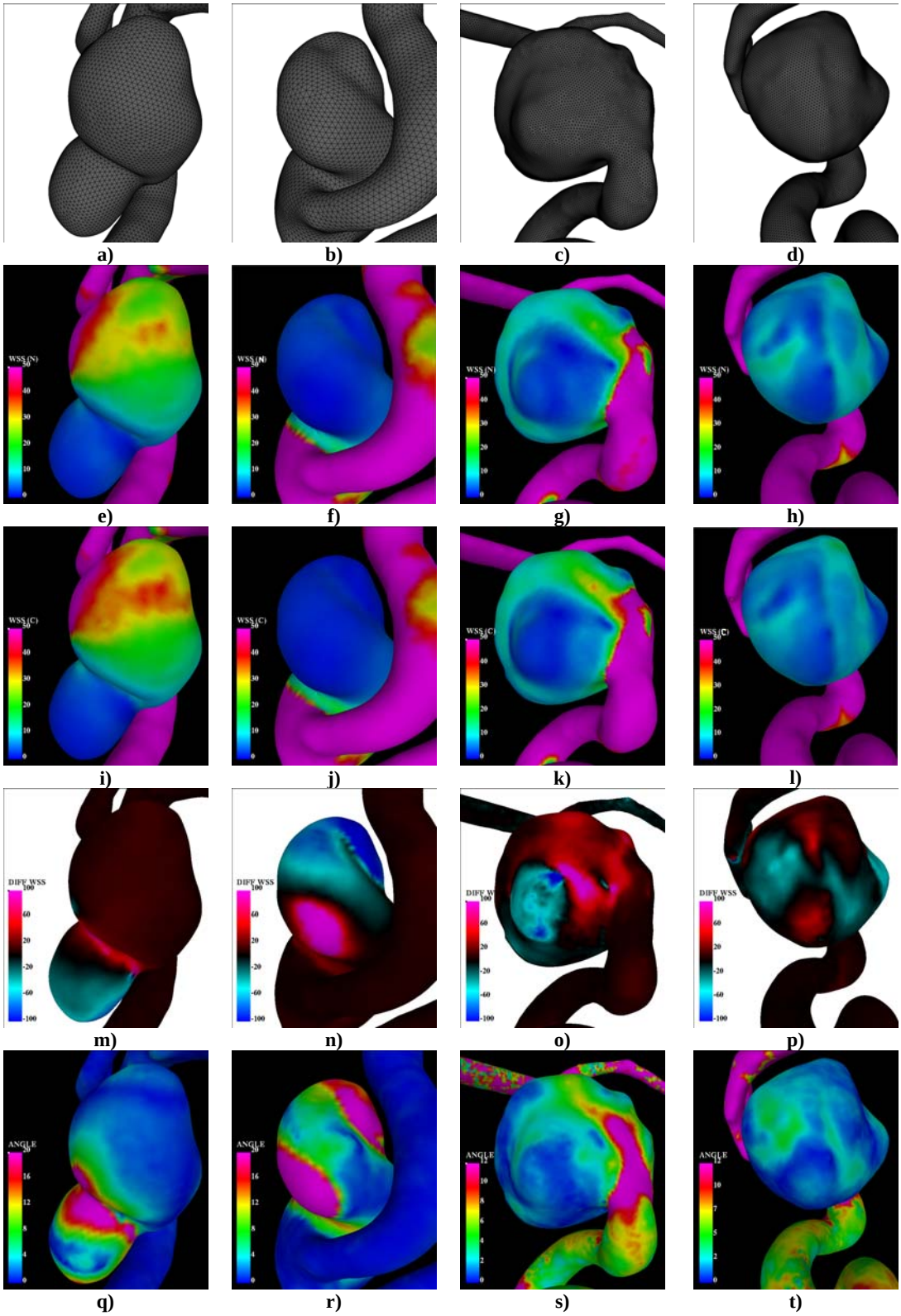

Figure 2: First and second columns correspond to the first case, and third and fourth column correspond to the second case. First row (a-d): vascular models; Second row (e-h): WSS maps for Newtonian rheology; Third row (i-l): WSS maps for Casson rheology; Fourth row (m-p): relative difference between the Newtonian and Casson WSS, where magenta indicates that Casson WSS is as much as twice the Newtonian WSS, blue indicates that Newtonian WSS is as much as twice the Casson WSS, and dark regions correspond to similar WSS values; Fifth row (q-t): difference in WSS vector orientation, where magenta represents a maximum of 15° for the first case, and 5° for the second case.

The first observation is that WSS distributions have similar characteristics for both rheologies. That result is in agreement with a previous sensitivity study (Cebral et al., 2005). The second observation is that large arteries, where greater flow rates are expected, have relatively larger WSS values for Casson model, which appears as dark red regions in Figures 2m-p. This fact is in line with theoretical results in simplified configurations and flow conditions (Mazumdar, 1981; Castro et al., 2008). The third observation is that not only WSS values differ between Newtonian and non-Newtonian rheologies, but also their vector orientation does, which is as large as 20° for Case #1, and 12° for Case #2. There is no clear correlation between regions with different WSS values, and regions where WSS vectors exhibit different orientations. While in one of the lobulations in Case #1 large angular differences are associated to regions where any of the rheologies predict larger WSS values than the other one (compare Figure 2n to Figure 1r), that is not the case for Case #2 (compare Figure 2o to Figure 2s) where vector fields have similar orientations despite their different magnitudes. Additionally, in the neck of one of the lobulations of Case #1, WSS vector orientations significantly differ in regions where WSS magnitude values do not. In the same case, one of the lobulations is under relatively high WSS, resulting in a Newtonian WSS roughly 20% higher than Casson WSS (compare Figures 2i and 2m). Finally there is no clear correlation either between low WSS regions and regions where any of the rheologies predict larger WSS values. Particularly, for Case #1 Casson WSS is significantly greater or less than Newtonian WSS in regions of low WSS (compared Figures 2f, 2j and 2n). The same fact is observed in Case #2, when comparing Figures 2g, 2k and 2o.

4 DISCUSION

The purpose of this work is to investigate the differences between Newtonian and Casson WSS characteristics under a pulsatile flow condition at aneurysm sac models reconstructed from angiographic images. Our results corroborate that the smallest differences take place in large arteries where the flow rate is also large (Mazumdar, 1981). Additionally, the WSS distributions do not exhibit significant differences when both rheologies are compared. This result is in line with a previous sensitivity study (Cebral et al., 2005).

The characteristics of a non-Newtonian flow for idealized vascular models harboring aneurysms have been investigated in the past (Low et. al, 1993; Khanafer et al., 2006; Fisher et al., 2009). When a stationary flow in a rigid and straight pipe is considered, WSS values are larger for a Casson flow than for a Newtonian rheology. This difference is more significant for low Reynold's numbers (Castro et al., 2008). However, when realistic geometries are considered under pulsatile regimes the differences must be investigated in a patient-specific basis. Rayz et al. found no significant differences between low wall shear stress regions that may be associated with risk of thrombus formation using Newtonian and non-Newtonian computational fluid dynamic simulations in three patients (Rayz et al., 2008). However, accounting for non-Newtonian behavior improved the agreement with observations using longitudinal MRI studies. Xiang et al. showed that Newtonian viscosity model could overestimate normalized wall shear stress and consequently underestimate the risk of rupture of intracranial aneurysm in three internal carotid artery saccular aneurysms (Xiang et al., 2012). These results would suggest a dependence of WSS distributions on the real vascular geometry. Fisher et al. studied a given number of rheologies in different idealized aneurysm models. It was found that spatially averaged Newtonian WSS was higher than the corresponding Casson WSS at the aneurysm dome during the whole cardiac cycle. The relative difference was higher during the diastole rather than the systole (Fisher et al., 2009).

The main finding in our work is that there is no clear correlation between low WSS regions and regions where any of the rheologies predict larger WSS values. Particularly, large relative differences between Casson and Newtonian WSS may appear in a low WSS region (<10 dyn/cm^2). It can also be observed that flow in the internal carotid artery produces little greater WSS values for the non-Newtonian rheology with similar vector orientations. Finally, a non negligible change in WSS vector orientation is observed which is as large as 20° in regions of low WSS. The location of those regions is not necessarily associated with regions where large differences in WSS occur when considering different rheologies. These observations may indicate that the realistic geometry plays an important role in the intra-aneurysmal hemodynamic characteristics, resulting in low flow regions where either the Newtonian or non-Newtonian WSS may be larger than the other one, exhibiting also differences in the vector orientation.

The methodology utilized has some limitations. First, only two cases were considered, therefore no statistical implications can be derived from these results. However, these findings show some discrepancy with respect to the results presented by Xiang et al. Second, although non-Newtonian behavior should be considered in certain vascular configurations, the Casson model, as well as other non-Newtonian models, is only a possible representation that not necessarily depicts in an accurate manner the intensity and distribution of blood internal forces (Fisher et al., 2009). Finally, the same mean WSS was imposed at the inlets of the models based on the principle of minimal work expressed by Murray's law (Sherman, 1981). Although that assumption is an approximation, it allows comparability when searching for associations between hemodynamic features and aneurysm risk of growth and rupture in large populations, and was used in previous works (Castro et al., 2006, Cebral et al., 2008, Cebral et al., 2011). Instead, Xiang et al. analyzed the WSS normalized with respect to the typical WSS values at the near parent artery (Xiang et al., 2012), which may affect comparability.

ACKNOWLEDGEMENTS

Marcelo A. Castro wants to acknowledge CONICET (Ministerio de Ciencia, Tecnología e Innovación Productiva, Argentina) for financial support of this work.

REFERENCES

Castro, M.A., Putman, C.M., Cebral, J.R., Computational Fluid Dynamics Modeling of Intracranial Aneurysms: Effects of Parent Artery Segmentation on Intraaneurysmal Hemodynamics. *American Journal of Neuroradiology*, 27:1703-1709, 2006.

Castro, M.A., Putman C.M., Cebral, J.R., Computational Hemodynamics of cerebral aneurysms: Assessing the risk of rupture from hemodynamic patterns, *VDM Verlag*, ISBN 9783639094411, 2008.

Castro, M.A., Putman, C.M., Cebral, J.R., Hemodynamic Patterns of Anterior Communicating Artery Aneurysms: A Possible Association with Rupture. *American Journal of Neuroradiology*, 30(2):297-302, 2009.

Cebral, J.R., Castro, M.A., Appanaboyina, S., Putman, C., Millán, D., Frangi, A., Efficient Pipeline for Image-Based Patient-Specific Analysis of Cerebral Aneurysms Hemodynamics: Technique and Sensitivity. *IEEE - Transactions on Medical Imaging - Special Issue on Vascular Imaging*, 24(4):457-467, 2005.

Cebral, J.R., Castro, M.A., Putman, C.M., Alperin, N., Flow-area relationship in internal carotid and vertebral arteries. *Physiological Measurements*, 29(10):585-594, 2008.

Cebral, J.R., Sheridan, M., Putman, C.M., Hemodynamics and Bleb Formation in Intracranial Aneurysms. *American Journal of Neuroradiology*, 31:304-310, 2010.

Cebral, J.R., Mut, F., Weir, J., Putman, C.M., Quantitative characterization of the hemodynamic environment in ruptured and unruptured brain aneurysms. *American Journal of Neuroradiology*, 32:145-151, 2011.

Crompton, M., Mechanisms of growth and rupture in cerebral berry aneurysms. *British Journal of Medicine*, 1:1138-1142, 1966.

Fisher, C., Stroud Rossmann, J., Effects of non-Newtonian behavior on hemodynamics of cerebral aneurysms, *Journal of Biomechanical Engineering*, 31:1-9, 2009.

Ford, M.D., Hoi, Y., Piccinelli, M., Antiga, L., Steinman, A.D., An objective approach to digital removal of saccular aneurysms: Technique and applications. *The British Journal of Radiology*, 82:56-61, 2009.

Jou, L.D., Lee, D.H., Morsi, H., Mawad, M.E., Wall Shear Stress on Ruptured and Unruptured Intracranial Aneurysms at the Internal Carotid Artery. *American Journal of Neuroradiology*, 29:1761-1767, 2008.

Khanafer, K.M., Gadhoke, P., Berguer, R., Bull, J.L., Modeling pulsatile flow in aortic aneurysms: Effect on non-Newtonian properties of blood, *Biorheology*, 43:661-679, 2006.

Kulcsar, Z., Ugron, A., Marosfo, M., Berentei, Z., Paal, G., Szikora, I., Hemodynamics of Cerebral Aneurysm Initiation: The Role of Wall Shear Stress and Spatial Wall Shear Stress Gradient. *American Journal of Neuroradiology*, 32(3):587-594, 2011.

Löhner, R., Extensions and improvements of the advancing front grid generation technique. *Computational Methods in Applied Mechanical Engineering*, 5:119–132, 1996a.

Löhner, R., Regridding surface triangulations. Journal of Computational Physics, 126:1–10, 1996b.

Löhner, R., Automatic unstructured grid generators. *Finite Elements Analysis Design*. 25:111–134, 1997.

Low, M., Perktold, K., Raunig, R., Hemodynamics in rigid and distensible saccular aneurysms: A numerical study of pulsatile flow characteristics, *Biorheology*, 30:287-298, 1993.

Mazumdar, J.N., Biofluid Mechanics, *World Scientific*, Singapore, 1992.

Nakatani, H., Hashimoto, N., Kang, H., Yamazoe, N., Kikuchi, H., et al., Cerebral blood flow patterns at major vessel bifurcations and aneurysms in rats. *Journal of Neurosurgery*, 74:258-262, 1991.

Pham, T.V., Mitsoulis, E., Entry and exit flows of Casson fluids, *Canadian Journal of Biomechanical Engineering*, 72:1080-1084, 1994.

Rayz V.L., Boussel, L., Lawton M.T., Acevedo-Bolton G., Ge L., Young W.L., Higashida R.T., Saloner D., Numerical modeling of the flow in intracranial aneurysms: Prediction of regions prone to thrombus formation, *Annals of Biomedical Engineerings*, 36:1793-1804, 2011.

Sherman, T.F. On connecting large vessels to small. The meaning of Murray's law. *J Gen Physiol.*, 78:431–453, 1981.

Shojima, M., et al., Magnitude and role of wall shear stress on cerebral aneurysm. Computational fluid dynamic study of 20 middle cerebral aneurysms. *Stroke*, 35:2500-2505, 2004.

Shojima, M., Nemoto, S., Morita, A., Oshima, M., Watanabe, E., Saito, N., Role of Shear Stress in the Blister Formation of Cerebral Aneurysms. *Neurosurgery*, 67(5):1268-1275, 2010.

Steinman, D.A., Milner, J.S., Norley, C.J., Lownie, S.P., Holdsworth, D.W. Image-based computational simulation of flow dynamics in a giant intracranial aneurysm. *Am J Neurorad*, 24(4):553-554, 2003.

Taylor, C.A., Hughes, T.J.R., Zarins, C.K., Finite element modeling of blood flow in arteries. *Computational Methods in Applied Mechanical Engineering*, 158:155–196, 1998.

Womersley, J.R., Method for the calculation of velocity, rate of flow and viscous drag in arteries when the pressure gradient is known. *J Physiol*, 127:553–563, 1955.

Yim, P.J., Vasbinder, B., Ho, V.H., et al., A deformable isosurface and vascular applications. In: Sonka M and Fitzpatrick JM, ed. Medical Imaging 2002: Image Processing, SPIE Vol. 4684. San Diego, Calif: SPIE; 1390–1397, 2002.